

Accuracy improvement of bulk optical polarization interferometric sensors

PAWEŁ WIERZBA, BOGDAN B. KOSMOWSKI

Gdańsk University of Technology, Faculty of Electronics, Telecommunication and Informatics,
Department of Optoelectronics, Narutowicza 11, PL-80952 Gdańsk, Poland

Interferometric sensors using bulk optical components exhibit very high measurement resolution. In order to attain high accuracy, these sensors are often implemented as polarization interferometers, in which stable and well-defined states of polarization are maintained. Unwanted phenomena degrading accuracy of this class of sensors are discussed in the paper. Signal processing technique which improves accuracy of polarization interferometric sensors is presented. Its implementation using analogue circuits is discussed and a method of improving its performance is devised.

Keywords: optical sensing, interferometry, polarization, displacement measurement, homodyne interferometers, nonlinearity reduction, polarization mixing, beamsplitters.

1. Introduction

Interferometric measurement methods have been an indispensable measuring tool used in an extensive range of applications (*e.g.*, [1–4]). This is due to their advantages, such as very high resolution and accuracy, ability to measure a broad range of quantities and relative ease of use. Setups performing interferometric measurements can be divided, according to the type of components used in their sensing part, into two groups: i) sensors with bulk optical components, ii) optical fibre sensors. Both groups of sensors share the same operating principles and basic analytical description. However, due to the difference in the properties of corresponding components used in setups belonging to each group (*e.g.*, bulk beamsplitters *vs.* 2×2 fibre couplers) and in description of light propagation in optical fibres and in free space, more detailed descriptions of these two groups differ considerably. Consequently, it is difficult to provide a concise unified description of both groups of sensors. Since the description of bulk optical sensors is more straightforward and is also the basis for description of optical fibre sensors, the following discussion covers interferometric bulk optical sensors. For comprehensive discussion of all aspects of implementation and operation of interferometric fibre optic sensors, refer to, *e.g.*, [4–6].

Often quoted advantages of interferometric sensors which use bulk optical components include: contactless operation, moderate requirements on the surfaces of investigated objects (no special pre-treatment is required) and very high measurement

resolution, which for displacement measurement is often better than 0.1 nm [7]. Accuracy of interferometric sensors is usually much lower than their resolution – about 1/100 of the operating wavelength λ . This is caused mainly by uncontrolled changes in the state of polarization of the source and drifts of polarization properties of optical components used in the interferometer.

Implementation of interferometric sensors using polarization interferometers, in which interfering beams have stable state of polarization, not only results in improved accuracy, but makes it possible to devise new configurations of increased sensitivity (*cf.* [8] and Fig. 7b) or improved tolerance to misalignment. In order to maintain stable and well-defined states of polarization, polarization interferometric sensors use polarizing beamsplitters or birefringent prisms, optical components which do not modify the states of polarization of interfering beams and the source which has stable power, wavelength and state of polarization.

Polarization interferometric sensors can perform absolute [9] and relative [10] distance measurement, birefringence measurement [11], surface roughness measurement [12] (*i.e.*, optical profilometry) and wavelength measurement [13]. Moreover, they can be incorporated into other precise measuring instruments, such as atomic force microscope (AFM) [14]. Finally, polarization interferometric sensors are often used for indirect measurement of several physical quantities (*e.g.*, pressure, temperature, refractive index) whose changes can be converted into changes of optical path length.

An example of polarization interferometric sensor is presented in Fig. 1. Light from a single frequency laser, linearly polarized at 45° to the plane of the figure, is split by the polarizing beamsplitter PBS into the measurement beam, polarized in the plane of the figure, and the reference beam, polarized perpendicularly to that plane. Subsequently, the beams are reflected by retroreflectors and recombined in PBS. Phase difference between the beams is proportional to the optical path length difference between measurement and reference arms. On entering the detection setup each beam

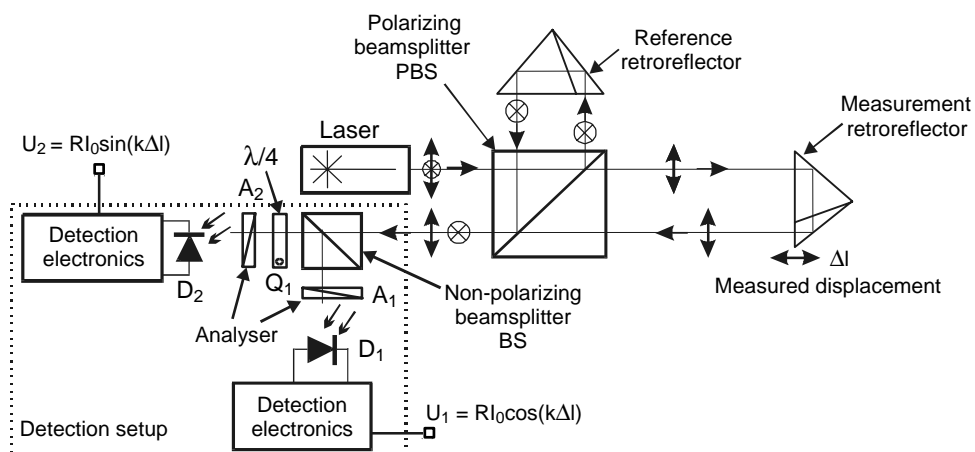


Fig. 1. Displacement sensor using polarization interferometer and quadrature detection.

is divided by the non-polarizing beamsplitter BS into two channels. In the first channel the beams are brought to interference on detector D_1 by polarizer A_1 whose axis is aligned at 45° to the plane of the figure. In the second channel, additional phase difference of 90° is introduced between the reference and measurement beams using quarter-wave plate Q_1 placed in front of polarizer A_2 bringing the beams to interference on detector D_2 .

Intensity of light reaching detectors D_1 and D_2 can be expressed as $I_1 = I_0/2[1 + \cos(k\Delta l)]$ and $I_2 = I_0/2[1 + \sin(k\Delta l)]$, respectively, where I_0 – maximum intensity on a detector, k – wavenumber ($k = 2\pi/\lambda$), Δl – measured displacement. By means of simple operations on analog signals from the detectors, two electrical signals, U_1 and U_2 , are obtained which are functions of Δl :

$$\begin{aligned} U_1 &= RI_0 \cos(k\Delta l), \\ U_2 &= RI_0 \sin(k\Delta l) \end{aligned} \tag{1}$$

where R is sensitivity of the detection setup. Using U_1 and U_2 and knowing wavenumber k , value of Δl can be calculated. As signals U_1 and U_2 are shifted by 90° with respect to each other, the direction of Δl changes can always be determined.

In many particular applications custom polarization interferometric sensors must be developed which perform these measurements with high resolution and accuracy. In order to accomplish this task, it is vital to have a good understanding of factors affecting accuracy and stability of these sensors, as discussed in the following section. The possibility of applying correction methods that greatly reduce nonlinearity of polarization interferometric sensors, also discussed there is very beneficial, too. These methods can be used with most polarization interferometric sensors, although they were originally developed for displacement measurement metrology. Because a large portion of these sensors is implemented as homodyne interferometers, the following discussion is restricted to that class of interferometers.

2. Nonlinearity sources in polarization interferometric sensors

The accuracy of homodyne polarization interferometric sensors is decreased as a result of several parasitic phenomena, of which the most important are: i) polarization cross-talk (Fig. 2a), ii) parasitic birefringence of components (Fig. 2b and c), iii) finite extinction ratio of components (Fig. 2d) and iv) reflections at glass–air interfaces (Fig. 2e).

Polarization cross-talk (Fig. 2a) occurs when part of linearly polarized light beam (E_x or E_y) is coupled to the orthogonal beam (E_{xo} or E_{yo} , respectively) becoming a parasitic component (E_{px} or E_{py} , respectively) of this beam. Present in waveplates, polarizing beamsplitters and polarizing prisms (*e.g.*, Wollaston or Nomarski prisms), this phenomenon is caused by misalignment between the direction of the optical axis in these components and polarization plane of beams E_x or E_y . When E_x or E_y are reference and measurement beams of a polarization interferometer, polarization

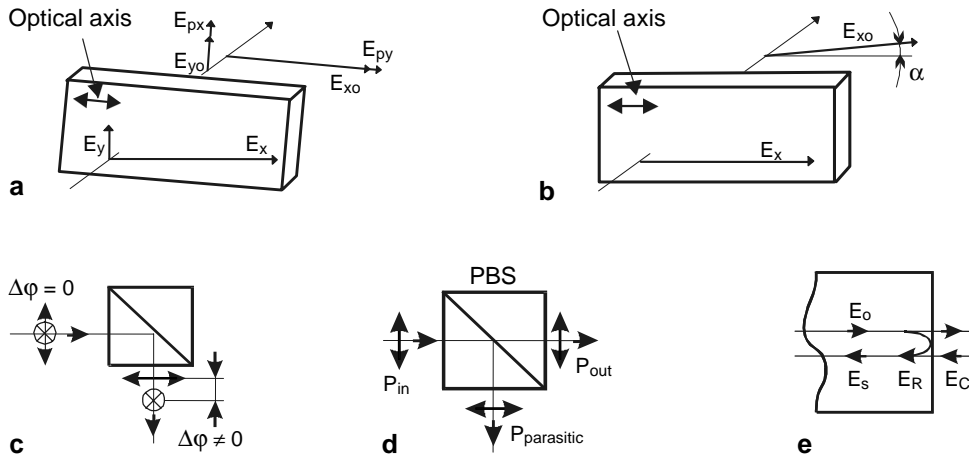


Fig. 2. Phenomena affecting accuracy of homodyne polarization interferometers polarization cross-talk (a), parasitic birefringence (b and c), finite extinction ratio (d), reflections at glass-air interface (e).

cross-talk introduces a phase shift between them, which is an important source of errors in polarization interferometric sensors.

Parasitic birefringence exists in optical elements, such as non-polarizing beamsplitters, waveplates, retroreflectors or Dove prisms, affecting the state of polarization of light propagating through them. When circular birefringence (*i.e.*, optical activity) is present in an element, the plane of polarization of light incident on it is rotated through an angle α , as shown in Fig. 2b. When linear birefringence is present in an element and its optical axis is parallel to one of orthogonal components of the light beam, a phase shift is introduced between them, as shown in Fig. 2c. Otherwise, polarization cross-talk occurs, as described above.

Polarizing beamsplitters and polarizing prisms, such as Wollaston or Nomarski prisms, should divide a light beam incident on them into two beams linearly polarized in orthogonal planes. Therefore, the beam incident on the polarizing beamsplitter PBS shown in Fig. 2d should propagate across it. In fact, a small amount of power is coupled out to the other direction (downwards in Fig. 2d). Extinction ratio e can be defined as the ratio of power transmitted in the right direction P_{out} to power $P_{\text{parasitic}}$ coupled into the other direction, *i.e.*, $e = P_{\text{out}}/P_{\text{parasitic}}$. Ideal beamsplitters and polarizing prisms have infinite extinction ratio, due to $P_{\text{parasitic}} = 0$. In real components this parameter ranges from 10^4 to 10^6 .

Another source of inaccuracy of polarization interferometric sensors is Fresnel reflection at the surfaces of optical components (*e.g.*, glass-air, glass-vacuum or plastic-air interfaces). When a beam having amplitude E_o crosses such an interface (either entering or leaving a component), part of its power is reflected back. Reflected beam, whose amplitude E_R depends on refractive index difference between air and the material of the optical component, can combine with another beam E_C propagating in the same direction, as shown schematically in Fig. 2e. Assuming that the beams are

coherent and have the same state of polarization, amplitude E_S of their superposition can be expressed as:

$$E_S = E_C + E_R \exp(j\varphi) \quad (2)$$

where φ – phase difference between beams E_R and E_C . This phenomenon can be seen as an unwanted phase modification imparted on beam E_C by reflected beam E_R . When phase difference φ is a function of the measured quantity, this is an important source of errors in optical setups in which beams E_o and E_c overlap, *e.g.*, in Michelson interferometers.

Apart from measurement errors caused by the phenomena present in optical components and described above, additional errors are introduced by the electronic part of the detection setup. Most often these errors take the form of voltage offsets present at the outputs of the setup or gain mismatch between the two outputs.

All these phenomena manifest themselves as periodical nonlinearity of polarization interferometric sensors. According to description introduced in [15], distorted output signals U_{1d} and U_{2d} can be expressed in terms of undistorted output signals U_1 and U_2 , given by Eq. (1), as:

$$\begin{aligned} U_{1d} &= U_1 + p, \\ U_{2d} &= \frac{1}{r}(U_2 \cos \alpha - U_1 \sin \alpha) + q \end{aligned} \quad (3)$$

where r – gain ratio of the two channels ($r = G_1/G_2$), p – offset in the first channel, q – offset in the second channel, α – quadrature error.

Lissajous figure of U_{1d} and U_{2d} is an ellipse, randomly distorted by the presence of noise in U_{1d} and U_{2d} , as shown in Fig. 3. In an ideal system, gains of both channels are equal (*i.e.*, their ratio $r = 1$), no offsets are present ($p = q = 0$) and phase difference between the channels is 90° (*i.e.*, $\alpha = 0$), therefore Eq. (3) reduces to Eq. (1) and Lissajous figure of U_{1d} and U_{2d} becomes a circle.

Performing the least-square fitting of Eq. (3) to measurement data acquired for the range of $k\Delta l$ greater than 2π , values of r , p , q and α can be found. Subsequently, undistorted output signals U_1 and U_2 can be calculated from Eq. (3), rewritten as:

$$\begin{aligned} U_1 &= U_{1d} - p, \\ U_2 &= \frac{1}{\cos \alpha} [(U_{1d} - p) \sin \alpha + r(U_{2d} - q)]. \end{aligned} \quad (4)$$

Correction procedure described above is a very time-consuming process, in which the most computation-intensive task is calculation of r , p , q and α by the least-square fitting. Since Eq. (3) must remain fitted to data being processed, all parameters have to be recalculated each time any one of them changes. In order to avoid frequent

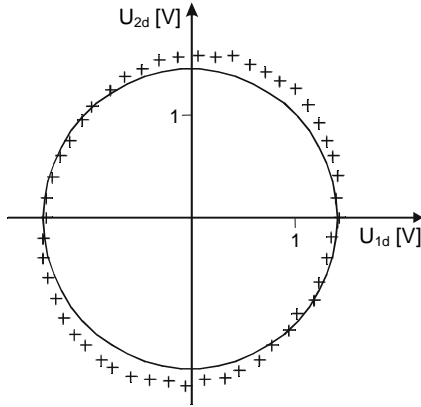


Fig. 3. Lissajous figure of ideal (—) and real (+) phase quadrature signals from a polarization interferometer.

recalculations, the sensor should have low drift of polarization properties of its elements, small dependence of these properties on the instantaneous value of measured quantity as well as low noise and drifts in detection electronics.

Correction of measurement data can be performed either off-line, when data are acquired and stored first and the correction process is performed afterwards, or on-line, *i.e.*, during data acquisition. Off-line correction is performed in digital domain, using a PC or dedicated DSP hardware, often after passing the data through a digital noise filter. On-line correction, which is much more difficult to perform due to time constraints, can be carried out either in digital domain, using a high-throughput DSP system [16] or in a mixed-signal mode, by performing the fitting in digital domain, converting values of calculated parameters into voltages using D/A converters, and feeding these voltages to an analog circuit performing the correction in analog domain [9]. The latter method can reduce the amount of calculations, and when frequent recalculations of ellipse parameters are not required, it may obviate the need to use a high-throughput DSP system.

An example of circuit for correcting output signals U_{1d} and U_{2d} from a polarization interferometer is presented in Fig. 4. Its transfer function can be written as:

$$\begin{aligned}
 U_1 &= \frac{U_{1d}U_{Gx}}{K} + U_{Ox}, \\
 U_2 &= \frac{U_{Gy}}{K} \left[\frac{U_{1d}U_{\phi}}{K} - kU_{1d} + U_{2d} \right] + U_{Oy}
 \end{aligned}
 \tag{5}$$

where K – scale factor of the multipliers, U_{Gx} and U_{Gy} – voltages controlling gain of the first and second channel, respectively, U_{Ox} and U_{Oy} – voltages controlling offset of the first and second channel and U_{ϕ} – voltage controlling phase difference between the two channels. Comparing Eq. (5) with Eq. (3), values of U_{ϕ} , U_{Gx} , U_{Gy} , U_{Ox} and U_{Oy} can be expressed in terms of ellipse parameters r , p , q and α .

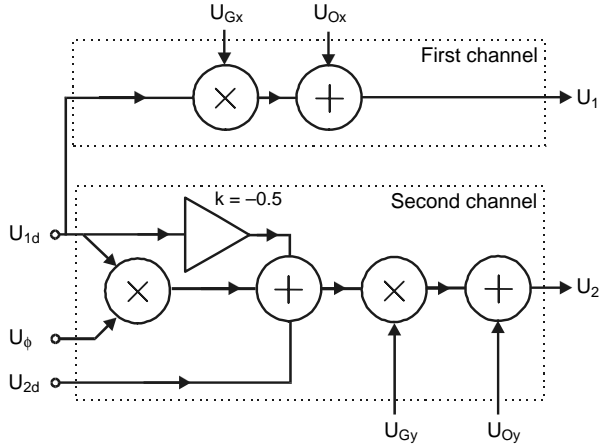


Fig. 4. Example implementation of nonlinearity correcting circuit.

Nonlinearity reduction up to 18 times was demonstrated using the circuit from Fig. 4 by authors of [9]. Further reduction seems to be possible by decreasing nonlinearity of the correction circuit by addressing its most important source – multipliers. Since the range of U_ϕ , U_{Gx} and U_{Gy} is limited (*i.e.*, $\Delta U/U \leq 1$) for all practical circuits, it is possible to use an elegant solution due to PEASE [17] in which most of the gain is obtained with a linear amplifier, and a multiplier is used only to adjust it over required range. In the following section we present our solution employing this technique.

3. Improved analog correction circuit

First, let us consider the first channel of correction circuit presented in Fig. 4. We can safely assume that required gain range in this circuit is 0.8 to 1.2 (*i.e.*, $\pm 20\%$ change around nominal value 1.0), that U_{1d} varies from -5 to $+5$ V and that maximum voltage at any multiplier input can range from -10 to $+10$ V, while its output voltage can be from -12 to $+12$ V.

We can replace the first channel of this circuit with the circuit presented in Fig. 5, where γ is the division ratio of the resistive divider. The transfer function of the latter circuit can be expressed as:

$$U_1 = \left[1 + G_2 \frac{U_{Gx}}{K} \frac{1}{\gamma} \right] U_{1d} + U_{Ox}. \quad (6)$$

Since the amplitude of input signal U_{1d} is 5 V and maximum voltage allowed on the multiplier is 10 V, G_2 can be set to 2V/V. As in most cases $|U_{Gx}/K| \leq 1$, division ratio γ needed to obtain $\pm 20\%$ gain change is 10. It should be noted that any nonlinearity observed at the output of the multiplier is also divided by 10. Therefore,

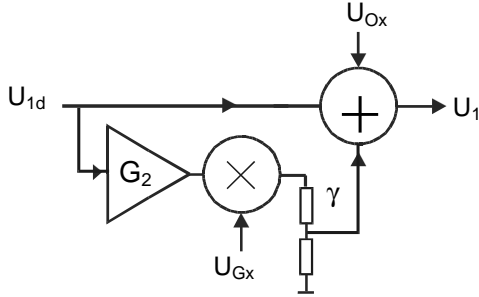


Fig. 5. First channel of correcting circuit after modification.

a nonlinearity reduction by one order of magnitude, compared to the first channel of the circuit from Fig. 4, can be attained.

Second, let us start modification of the second channel of the circuit from Fig. 4 by rewriting its transfer function, which can be expressed using Eq. (4) as:

$$\begin{aligned} U_2 &= \tan \alpha U_{1d} + \frac{r}{\cos \alpha} U_{2d} - \left[p \tan \alpha + \frac{r}{\cos \alpha} q \right] \\ &= \tan \alpha U_{1d} + \frac{r}{\cos \alpha} U_{2d} + U_{Oy}. \end{aligned} \quad (7)$$

The transfer function of the circuit from Fig. 6 is:

$$U_2 = \left[G_1 \frac{U_\phi}{K} \frac{1}{\gamma_1} \right] U_{1d} + \left[1 + G_2 \frac{U_{Gy}}{K} \frac{1}{\gamma_2} \right] U_{2d} + U_{Oy}. \quad (8)$$

Comparing Eq. (7) with Eq. (8), we can write:

$$\begin{aligned} \tan \alpha &= G_1 \frac{U_\phi}{K} \frac{1}{\gamma_1}, \\ \frac{r}{\cos \alpha} &= 1 + G_2 \frac{U_{Gy}}{K} \frac{1}{\gamma_2}, \\ U_{Oy} &= - \left[p \tan \alpha + \frac{r}{\cos \alpha} q \right]. \end{aligned} \quad (9)$$

Let us assume that U_{1d} and U_{2d} vary from -5 to $+5$ V, required gain ratio r can change from 0.8 to 1.2, $|\alpha| \leq 15^\circ$, and that maximum voltage at any multiplier input can be between -10 and $+10$ V while its output voltage can range from -12 to $+12$ V.

Gains G_1 and G_2 can be set to 2V/V since the amplitude of input signals U_{1d} and U_{2d} is 5 V and maximum voltage allowed on the multiplier is 10 V. For the given range

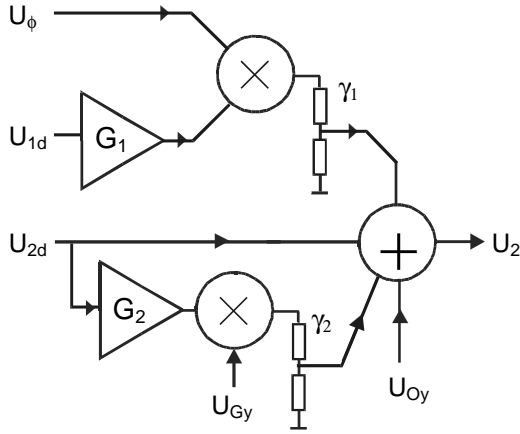


Fig. 6. Second channel of correcting circuit after modification.

of α we have $|\tan \alpha| \leq 0.268$ and $0.800 \leq (r/\cos \alpha) \leq 1.242$. Using these values in Eq. (9), together with the fact that $|U_{Gy}/K| \leq 1$ and $|U_\phi/K| \leq 1$, we arrive at:

$$G_1 \frac{1}{\gamma_1} \leq 0.268, \quad G_2 \frac{1}{\gamma_2} \leq 0.242, \quad (10)$$

from which division ratios γ_1 and γ_2 can be calculated:

$$\gamma_1 = 7.463, \quad \gamma_2 = 8.764. \quad (11)$$

It should be noted again that any nonlinearity present at the outputs of the multipliers is divided by γ_1 and γ_2 . Therefore, in the worst case, nonlinearity reduction in the second channel is over seven times ($\gamma_1 = 7.46$).

Finally, let us compare the complexity of the circuit from Fig. 4 with that of our modified circuit from Figs. 5 and 6. Assuming that summation points are implemented using an operational amplifier, which is usually the case, the latter circuit contains the same number of multipliers and only one operational amplifier more than the former circuit. Therefore, the cost of the latter circuit is only marginally higher than that of the original one.

In conclusion, the circuit presented in Figs. 5 and 6 offers nonlinearity improvement which is over seven times compared to the original circuit from Fig. 4. Moreover, this considerable improvement is obtained with only small additional complication of the circuit.

The method discussed can be used in sensors employing other, more sophisticated detection setups, such as the four-detector setup presented in Fig. 7 or the setup shown in Fig. 8 [18].

Operation of the balanced-quadrature detection setup from Fig. 7 is similar to that of detection setup presented in Fig. 1. On entering the setup, planes of polarization of

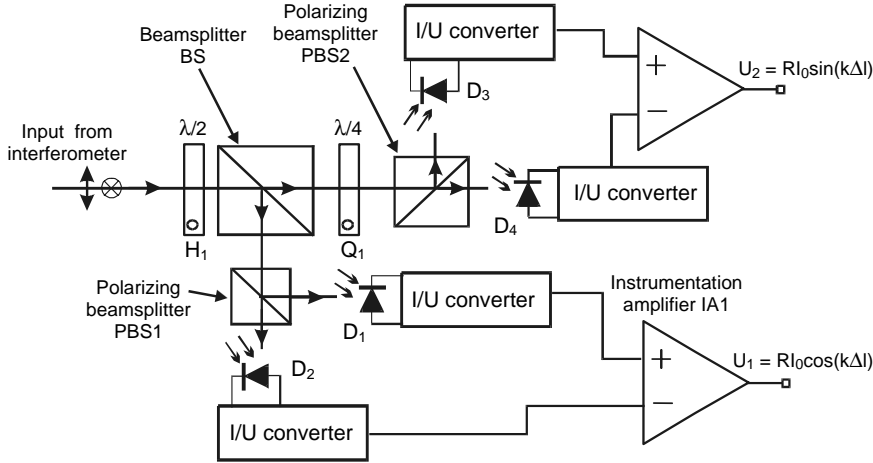


Fig. 7. Balanced quadrature detection setup.

reference and measurement beams are rotated by 45° using the halfwave plate H_1 . Then, each beam is divided by the non-polarizing beamsplitter BS into two channels. In the first channel, the beams are brought to interference on detectors D_1 and D_2 by the polarizing beamsplitter PBS1. In the second channel, additional phase difference of 90° is introduced between the reference and measurement beams using a quarter-wave plate Q_1 placed in front of the polarizing beamsplitter PBS2. This beamsplitter brings the beams to interference on detectors D_3 and D_4 . Signals from detectors D_1 – D_4 after I/U converters can be expressed as

$$\begin{aligned}
 U_{d1} &= \frac{1}{2} RI_0 [1 + \cos(k\Delta l)], & U_{d2} &= \frac{1}{2} RI_0 [1 - \cos(k\Delta l)], \\
 U_{d3} &= \frac{1}{2} RI_0 [1 + \sin(k\Delta l)], & U_{d4} &= \frac{1}{2} RI_0 [1 - \sin(k\Delta l)],
 \end{aligned}
 \tag{12}$$

Therefore, output signals of instrumentation amplifiers, giving directly the desired information can be expressed as:

$$\begin{aligned}
 U_1 &= U_{d1} - U_{d2} = RI_0 \cos(k\Delta l), \\
 U_2 &= U_{d3} - U_{d4} = RI_0 \sin(k\Delta l).
 \end{aligned}
 \tag{13}$$

The detection setup presented in Fig. 8a [18] uses a Nomarski prism, an analyser and a set of three photodiodes D_1 , D_2 and D_3 shown in Fig. 8b. Reference and measurement beams entering the setup are expanded by the beam expander BE and are incident on the Nomarski prism NP, whose optical axis is parallel to the

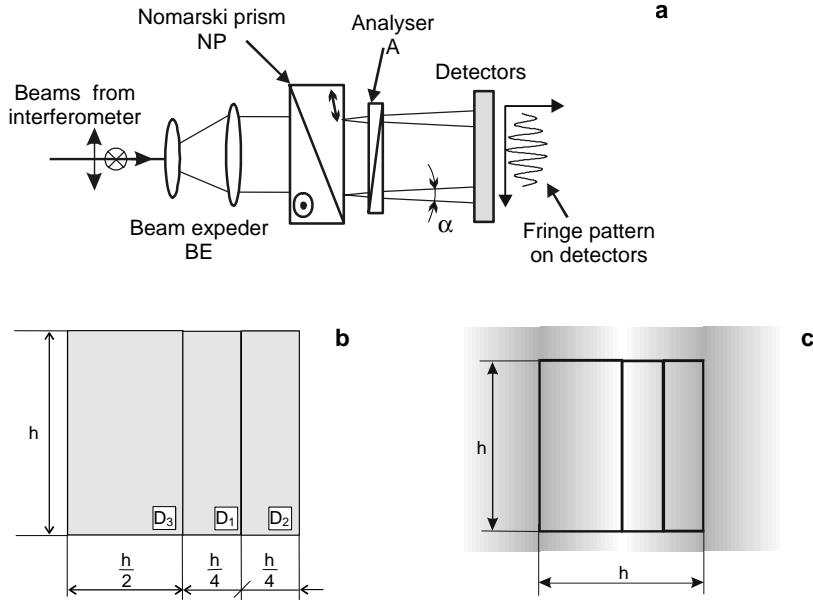


Fig. 8. Detection setup using Nomarski prism: view of the setup (a), dimensions of detectors (b), fringe pattern illuminating detectors (c); h – fringe spacing.

polarization plane of one of the beams. This prism changes propagation directions of reference and measurement beams, so that a small angle ($0.5\text{--}5^\circ$) α is introduced between the beams. The analyser A brings the two beams into interference, creating a fringe pattern on the photodiodes, as shown in Fig. 8c. Positions of dark and bright fringes depend on phase difference between the two beams.

Assuming that maximum intensity of the fringe pattern $I_{\max}(x, y)$ is constant across the surfaces of photodiodes (D_1, D_2, D_3), it can be shown that their currents i_1, i_2 and i_3 can be written as:

$$i_{\text{ref}} = i_1 + i_2 + i_3 = \text{const},$$

$$i_1 = \frac{i_{\text{ref}}}{4} \left[1 - \frac{2\sqrt{2}V}{\pi} \cos\left(k\Delta l + \frac{\pi}{4}\right) \right],$$

$$i_2 = \frac{i_{\text{ref}}}{2} \left[1 + \frac{2\sqrt{2}V}{\pi} \sin\left(k\Delta l + \frac{\pi}{4}\right) \right].$$
(14)

From Eqs. (14) it can be seen that in this case it is easier to obtain output signals proportional to $\sin(k\Delta l + \pi/4)$ and $\cos(k\Delta l + \pi/4)$, rather than to $\sin(k\Delta l)$ and $\cos(k\Delta l)$. These signals are obtained by:

$$\begin{aligned}
4i_1 - i_{\text{ref}} &= i_{\text{ref}} \frac{2\sqrt{2} V}{\pi} \cos\left(k\Delta l + \frac{\pi}{4}\right), \\
i_{\text{ref}} - 4i_2 &= i_{\text{ref}} \frac{2\sqrt{2} V}{\pi} \sin\left(k\Delta l + \frac{\pi}{4}\right)
\end{aligned}
\tag{15}$$

where V – visibility of fringes.

An important advantage of this setup is its simplicity and compact layout. Moreover, the setup does not use non-polarizing beamsplitters which can be an important source of polarization cross-talk and birefringence in detection setups.

4. Polarization interferometric sensors

The technique for nonlinearity reduction described above is used in several applications, such as surface roughness measurement, wavelength measurement, distance-measurement metrology as well as in AFM. It can be extended to other polarization interferometric sensors, such as hydrostatic pressure sensors (Fig. 9a) or relative displacement measurement sensors (Fig. 9b) [8]. Moreover, it can also be applied to waveguide polarimetric sensors for complex refractive index measurement, biosensing and immunosensing (Fig. 9c) [19].

Operation of hydrostatic pressure sensor presented in Fig. 9a is similar to that of the Michelson interferometer. Light from the source is divided by the Wollaston prism into the measurement beam, polarized in the plane of the figure and the reference beam polarized perpendicularly to the plane of the figure. Reflected from the pressure-sensing membrane, the beams return to the Wollaston prism, where they are combined. Phase difference between the orthogonal components of the resulting beam is proportional to the optical path length difference of reference and measurement arms. An important advantage of this sensor is that it is sensitive only to pressure-induced membrane deformation. Translation of the membrane, *e.g.*, induced by change of temperature, does not influence the measurement.

Relative displacement sensor, presented in Fig. 9b, which can also be used to measure hydrostatic pressure, is a four-pass sensor, *i.e.*, light travels four times in its arms. Input beam is divided by the Wollaston prism into the measurement beam, polarized in the plane of the figure and the reference beam polarized perpendicularly to the plane of the figure. Reflected from the measured object, the beams pass through a quarter-wave plate, are reflected from a mirror placed behind it and pass again through the plate. The axes of the plate are aligned in such a way that the beams change their polarizations into orthogonal ones, *i.e.*, the measurement beam becomes polarized perpendicularly to the plane of the figure and the reference beam becomes polarized in that plane. The beams fall on the measured object, then are reflected from it, and return to the Wollaston prism, where they are combined. An important advantage of this sensor is that it is sensitive only to relative displacement Δx , rather

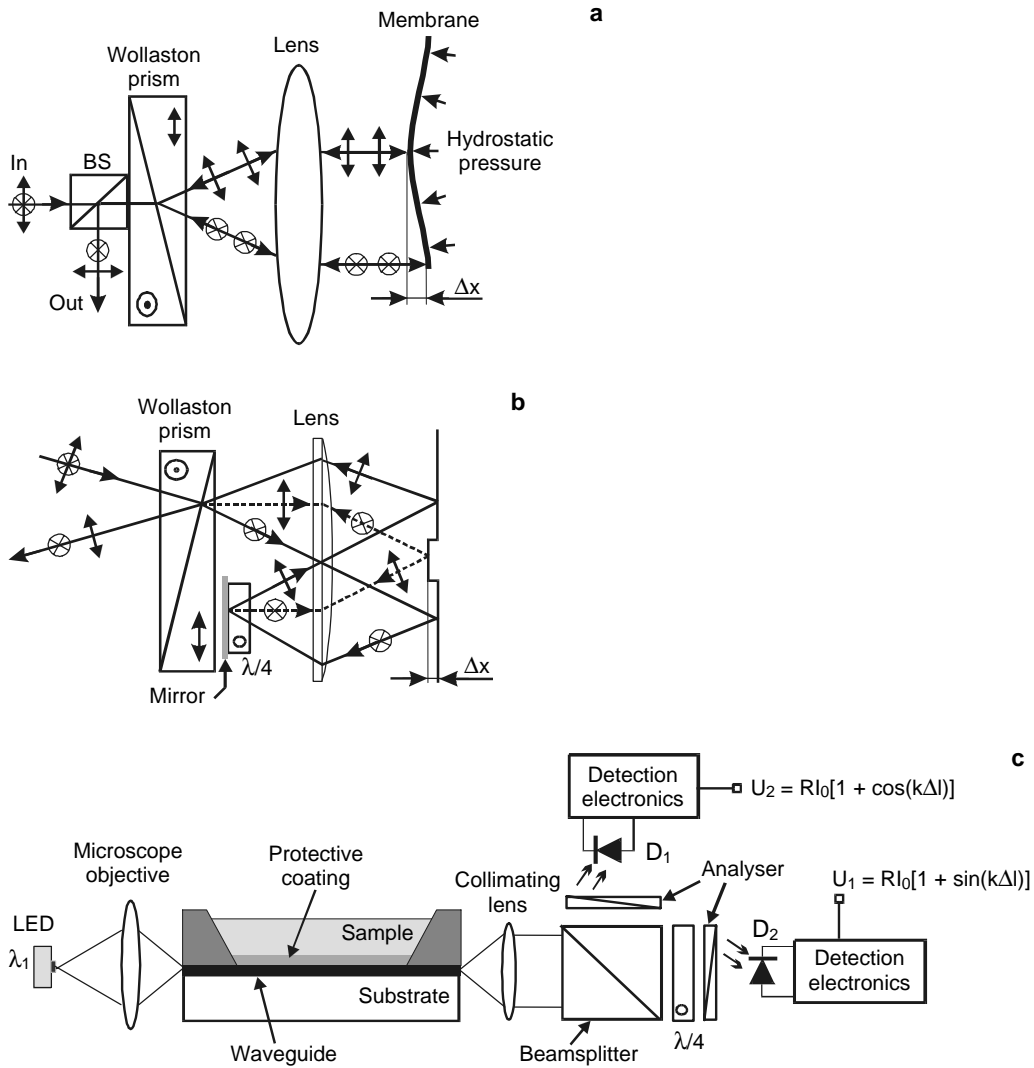


Fig. 9. Polarization interferometric sensors in which nonlinearity correction can be used: hydrostatic pressure sensor (a), relative displacement sensor (b), polarimetric waveguide sensor (c).

than to translation of measured object. Moreover, this sensor is not sensitive to small tilts of the surface of measured objects.

Complex refractive index sensor, presented in Fig. 9c, can also be used as a biosensor, in which an antigen-antibody interaction affects refractive index. Polarized light from the source is coupled into the sensing waveguide, where two polarization modes ${}_x\text{HE}_{11}$ and ${}_y\text{HE}_{11}$ are excited with equal amplitudes. Propagation constants of these modes are functions of refractive index of the sample (or antigen layer in

biosensors). Therefore, the value of refractive index can be obtained based on measured phase difference between polarization modes leaving the waveguide. This measurement is accomplished by the detection setup, in which the polarization modes are brought to interference by analysers.

5. Implementation issues

While polarization interferometric sensors combined with nonlinearity reduction technique described above are an attractive highly-accurate measuring tool, they exhibit certain disadvantages hindering their implementation. The most important problems are: excessive size of some optical setups, distortion of interfering wavefronts, difficult setting up due to reflections from the surfaces of lenses, difficulty to couple the sensors to a single-mode polarization-maintaining fiber as well as change of the wavefront shape as a function of displacement.

Excessive size is often encountered in sensors using a Wollaston or Nomarski prism in which spacing between sensing and reference beam is above 1 mm. The primary cause of this problem is small ($< 5\text{--}10^\circ$) splitting angle of the prism. A sensor similar to that from Fig. 9b, in which the transverse spacing of the beams is 2 mm, has overall length of optical setup over 60 mm [20]. Using Wollaston/Nomarski prisms with higher splitting angle (up to 30°) often requires more sophisticated focusing optics, such as multi-element assemblies containing aspheric lenses. Multiple lens surfaces give rise to a number of reflections on glass-air interfaces, making these setups difficult to align. Moreover, in such setups, wavefronts of measurement and reference beam are often distorted in a different way, which decreases interference contrast and makes these interferometers more sensitive to vibration.

Operation of polarization interferometric sensors may also be affected by change of the wavefront shape, caused by the change in the shape of measured surface. As illustrated in Fig. 9a, the measured hydrostatic pressure deforms the membrane in such a way that its surface becomes convex, modifying focal length of the system. As a result, the reflected measurement beam is no longer collimated (*i.e.*, it does not have a flat wavefront), which may affect the operation of the detection setup.

6. Conclusions

The accuracy of polarization interferometric sensors, which is often degraded by unwanted optical and electrical phenomena, can be improved by using a correction technique developed for metrology, based on adjustment of gain and removal of offsets in detection setup. Employing this technique it is possible to provide a real-time correction of measured data using analog or digital signal processing. Analog correction circuits can achieve accuracy much higher than demonstrated to date, by complementing multiplier-based variable gain stages with linear gain stages, as discussed in Sec. 3. Although some polarization interferometers are difficult to implement because of their size or complicated alignment, this class of sensors shows considerable application potential. Sensors employing optical components made from new crystalline and liquid crystal birefringent materials can potentially be made more compact and economical

at the same time offering high measurement accuracy. However, further research is needed on implementation of polarization interferometric sensors.

References

- [1] HARIHARAN P., *Interferometry with lasers* [In] *Progress in Optics*, [Ed.] E. Wolf, Vol. 24, Elsevier 1987, p. 104.
- [2] PLUTA M., *Advanced Light Microscopy*, Warszawa: PWN; Amsterdam, New York: Elsevier 1988.
- [3] BOBROFF N., *Recent advances in displacement measuring interferometry*, *Measurement Science and Technology* **4**(9), 1993, pp. 907–26.
- [4] JAROSZEWICZ L.R., *The role of polarization and coherence in fibre-optic interferometry*, MUT Warszawa 1995 (in Polish).
- [5] WOLIŃSKI T.R., *Polarimetric optical fibers and sensors* [In] *Progress in Optics*, [Ed.] E. Wolf, Vol. 15, Elsevier 2000, p. 1.
- [6] WOLIŃSKI T.R., *Polarization phenomena in optical systems* [In] *Encyclopedia of Optical Engineering* [Eds.] R. Barry Johnson, R.G. Diggers, Marcel Dekker Inc., New York 2003.
- [7] LAWALL J., KESSLER E., *Michelson interferometry with 10 pm accuracy*, *Review of Scientific Instruments* **71**(7), 2000, pp. 2669–76.
- [8] DYSON J., *Optics in a hostile environment*, *Applied Optics* **7**, 1968, p. 569.
- [9] EOM T., KIM J., JEONG K., *The dynamic compensation of nonlinearity in a homodyne laser interferometer*, *Measurement Science and Technology* **12**(10), 2001, pp. 1734–8.
- [10] LIU C., CLEGG W., LIU B., *Ultra low head-disk spacing measurement using dual-beam polarization interferometry*, *Optics and Laser Technology* **32**(4), 2000, pp. 287–91.
- [11] INDEBETOUW G., KLYSUBUN P., *Measurement of induced birefringence in film samples using a balanced polarization ring interferometer*, *Optics Communications* **151**(4-6), 1998, pp. 203–6.
- [12] GLEYZES P., LORLETTE V., SANT-JALMES H., BOCCARA A.C., *Roughness measurements in the picometric range using a polarization interferometer and a multichannel lock-in detection technique*, *International Journal of Machine Tools and Manufacture* **38**(5-6), 1998, pp. 715–7.
- [13] JUNCAR P., PINARD J., *Instrument to measure wave numbers of CW and pulsed laser lines: the sigmameter*, *Review of Scientific Instruments* **53**(7), 1982, pp. 939–48.
- [14] SCHONENBERGER C., ALVARADO S.F., *A differential interferometer for force microscopy*, *Review of Scientific Instruments* **60**(10), 1989, pp. 3131–4.
- [15] HEYDEMANN P.L.M., *Determination and correction of quadrature fringe measurement errors in interferometers*, *Applied Optics* **20**(19), 1981, pp. 3382–4.
- [16] DEI G., POHLENZ F., DANZEBRINK H.-U., HASCHKE K., WILKENING G., *Improving the performance of interferometers in metrological scanning probe microscopes*, *Measurement Science and Technology* **15**(2), 2004, pp. 444–50.
- [17] PEASE B., *What's all this multiplication stuff, anyhow?*, *Electronic Design*, August 1991, p. 121.
- [18] WIERZBA P., *Modelling of polarimetric sensors for applications in road traffic monitoring systems*, Ph.D. Thesis, Gdansk University of Technology 2000, p. 78 (in Polish).
- [19] GNYBA M., WIERZBA P., PLUCINSKI J., *Application of sol-gel-developed integrated optic devices to biochemical fiber optic sensors based on polarimetric interferometry*, *Proceedings of SPIE* **5505**, 2004, pp. 78–83.
- [20] WIERZBA P., *Optical Hydrophones*, VTT Technical Research Centre of Finland Internal Research Report, Oulu, Finland 2001.

*Received August 18, 2004
in revised form January 12, 2005*